Macromolecules
ARTICLE

Macromolecules **2010**, *43*, 7839–7844 **7839**
DOI: 10.1021/ma101132n

Dissipative Particle Dynamics Studies on Microstructure of pH-Sensitive Micelles for Sustained Drug Delivery

Xin Dong Guo, Li Juan Zhang, Zhi Min Wu, and Yu Qian*

School of Chemistry and Chemical Engineering, South China University of Technology, Guangzhou, 510640 P. R. China

Received May 21, 2010; Revised Manuscript Received July 15, 2010

ABSTRACT: Dissipative particle dynamics simulations were performed to study the microstructures of doxorubicin (DOX) loaded/blank micelles self-assembled from cholesterol conjugated $His_{10}Arg_{10}$ (HR20-Chol) at different pH conditions. DOX molecules can be efficiently encapsulated in the core of micelles. At pH > 6.0, these micelles have stronger DOX loading ability due to the hydrophobicity of histidine residues, as compared to that of pH < 6.0. With the decrease of pH from pH > 6.0 to pH < 6.0, the structure of micelles trends to be swelling from dense conformations. This structural transformation can facilitate the release of DOX from the core of micelles. All the simulation results are qualitatively consistent with the experimental results, demonstrating that the DPD method may provide a powerful tool in analysis and design of drug delivery systems.

1. Introduction

In recent years, polymeric micelles hold a significant potential as drug delivery vehicles for a wide array of anticancer drugs due to their unique properties, such as high solubility, high drug loading capacity, and low toxicity.[1−7] Especially, the pH-sensitive micelles were investigated as smart drug delivery systems for cancer therapy.[8−13] These micelles showed noticeable pH-dependent behavior, leading to a quick release at pH 5.0 and a slow release at pH 7.4. Although pH-sensitive micelles have been extensively studied, it is still highly demanded to understand the mechanism of controlling the drug releasing rate by pH conditions.

Computer simulations have emerged as a powerful tool in the study of the microstructures of amphiphilic copolymers in the past a few years.[14−22] Atomistic simulations could be used to analyze the molecular structure and dynamics behavior of molecules. However, they are limited in the time and length scales and difficult to observe the phase transformation process on a mesoscopic scale. Coarse-grained models were established to study the drug diffusion from core−shell nanoparticles.[23−25] Dissipative particle dynamics (DPD), introduced by Hoogerbrugge and Koelman[26] and revised by Español and Warren,[27] was used to simulate soft spherical particles interacting through a simple-wise potential and thermally equilibrate through hydrodynamics on a mesoscopic scale.[28] Groot and Warren[29,30] made an important contribution on this method by establishing a relationship between a simple function form of conservative repulsion in DPD and the Flory−Huggins parameter theory, which led to the DPD method being widely applied in the study of mesostructures of complex systems.[31−33] Zhong et al.[34−37] did a lot of work on the mesostructures of nanoparticles self-assembled from amphiphilic polymers using DPD simulations. Recently, Loverde et al.[38] refined and extended DPD methods that are suited to long time scales and long polymer chains. In addition, Valeriy et al.[39] studied the thermodynamics of the interaction of nanoparticles with cell membranes with a mesoscale thermodynamics model, which addressed thermodynamics aspects of the particle/membrane interactions. They have also suggested a better simulation method, the DPD method, which can provide more detailed information on the microstructures of drug and gene delivery systems. However, the pH-sensitivity of micelles which can be used for delivering drugs has seldom been studied via DPD simulations.

In our previous work, DPD simulations were performed to investigate the effect of composition,[40] solvents,[41] and PLA chirality[42] on the microstructures of drug delivery systems. In this work, it was extended to study the effect of pH values on the microstructures of doxorubicin (DOX) loaded/blank micelles self-assembled from cholesterol conjugated $His_{10}Arg_{10}$ (HR20-Chol), which has been successfully used for drug/gene delivery.[43,44] In solutions with different pH values, histidine residues present different forms because of the protonation of imidazole groups at pH lower than 6.0. Different forms lead to different interactions between them. In this work, the effect of pH value on the microstructures of drug loaded/blank micelles was investigated via DPD simulations, through which some mesoscopic information is obtained. In addition, to verify the correctness of the simulation results, experiments were also performed to characterize the critical micelle concentration and drug release behaviors.

2. Experimental Section

2.1. CMC Measurement. The critical micelle concentration (CMC) of peptides was estimated by fluorescence spectroscopy using pyrene as a probe. Briefly, a series of peptide solutions containing 0.616 μM pyrene were prepared at various concentrations (0−1.28 mg/mL) in PBS buffer (pH 5.0 or 7.4, 20 mM). Excitation spectra of solutions were recorded from 300 to 360 nm at room temperature, with an emission wavelength of 395 nm and bandwidth of 1 nm, using a spectrofluorometer (Fluorolog LFI 3751, Jobin Yvon Horiba, Edison, NY). The intensity ratios of I_{339} to I_{334} were plotted as a function of logarithm of peptide concentrations. The CMC value was taken from the intersection of the tangent to the curve at the inflection with the horizontal tangent through the points at low concentrations.

*Corresponding author: Tel +86-20-87113046, Fax +86-20-22236337, e-mail ceyuqian@scut.edu.cn.

Published on Web 07/30/2010

2.2. *In Vitro* DOX Release. The *in vitro* release profiles of DOX from micelles were studied using a dialysis bag (MWCO 1000 Da) at 37 °C. In order to acquire sink conditions, drug release studies were performed at low drug concentrations. Briefly, 3 mg of DOX loaded freeze-dried micelles was dispersed in 3 mL of the respective PBS buffer and allowed to stabilize for 30 min before being placed in a dialysis bag. The dialysis bag was then immersed in 50 mL of PBS solution (pH 5.0 or 7.4) in a beaker. The beaker was then placed in a 37 °C water bath and stirred at 100 rpm. The samples were drawn at desired time intervals and the drug concentration was analyzed using UV−vis spectrophotometry at 481 nm. The drug loading was calculated based on the standard curve obtained from DOX in the buffers. The *in vitro* release experiments were carried out in triplicate at each pH.

3. Simulation Methods

3.1. DPD Theory. Dissipative particle dynamics (DPD) is a stochastic simulation technique introduced by Hoogerbrugge and Koelman[26,28] and often used to simulate complex fluid dynamical behaviors. In the DPD method, the particles do not correspond to individual atoms or molecules, but to beads, which represent a group of atoms or a volume of fluid that is large on the atomistic scale but still macroscopically small.[26] All beads comply with Newton's equations of motion:[29,30]

$$\frac{\mathrm{d}\mathbf{r}_i}{\mathrm{d}t} = \mathbf{v}_i, \quad m_i\frac{\mathrm{d}\mathbf{v}_i}{\mathrm{d}t} = \mathbf{f}_i \tag{1}$$

where $\mathbf{r}_i$, $\mathbf{v}_i$, m_i, and $\mathbf{f}_i$ denote the position vector, velocity, mass, and total force on the particle i, respectively. For simplicity, the masses of all beads are set to 1 DPD unit.[29] The force between each pair of beads is a sum of a conservative force ($\mathbf{F}_{ij}^{\mathrm{C}}$), a dissipative force ($\mathbf{F}_{ij}^{\mathrm{D}}$), and a random force ($\mathbf{F}_{ij}^{\mathrm{R}}$):[27]

$$\mathbf{f}_i = \sum_{j\neq i}(\mathbf{F}_{ij}^{\mathrm{C}} + \mathbf{F}_{ij}^{\mathrm{D}} + \mathbf{F}_{ij}^{\mathrm{R}}) \tag{2}$$

The conservation force for nonbonded particles is defined by soft repulsion. The dissipative force corresponds to a frictional force that depends both on the position and relative velocities of the beads. The random force is a random interaction between a bead i and its neighbor bead j. All forces vanish beyond a certain cutoff radius, r_c, whose value is usually set to be 1 unit of length in simulations. The three forces are given by

$$\mathbf{F}_{ij}^{\mathrm{C}} = \begin{cases} a_{ij}(1-r_{ij})\hat{\mathbf{r}}_{ij} & (r_{ij} < 1) \\ 0 & (r_{ij} \geq 1) \end{cases} \tag{3}$$

$$\mathbf{F}_{ij}^{\mathrm{D}} = -\frac{\sigma^2(\omega(r_{ij}))^2}{2kT}(\mathbf{v}_{ij}\cdot\hat{\mathbf{r}}_{ij})\hat{\mathbf{r}}_{ij} \tag{4}$$

$$\mathbf{F}_{ij}^{\mathrm{R}} = \frac{\sigma\omega(r_{ij})\hat{\mathbf{r}}_{ij}\zeta}{\sqrt{\delta_t}} \tag{5}$$

where $\mathbf{r}_{\mathrm{ij}} = \mathbf{r}_{\mathrm{i}} - \mathbf{r}_{\mathrm{j}}$, $r_{ij} = |\mathbf{r}_{ij}|$, $\hat{\mathbf{r}}_{ij} = \mathbf{r}_{ij}/|\mathbf{r}_{ij}|$, $\mathbf{v}_{ij} = \mathbf{v}_i - \mathbf{v}_j$, k is the Boltzmann constant, T is the system temperature, σ is the noise strength and was set as 3 in our simulations, ζ is a randomly fluctuating variable with zero mean and unit variance, δ_t is time step of simulation, the r-dependent weight function $\omega(r) = 1 - r$ for $r < 1$ and $\omega(r) = 0$ for $r > 1$, and a_{ij} is the maximum repulsion between beads i and j. The parameter a_{ij} depends on the underlying atomistic interactions and is related to the Flory−Huggins (χ_{ij}) parameters through[30]

$$a_{ij} = a_{ii} + 3.27\chi_{ij} \tag{6}$$

Here, the values of χ_{ij} can be calculated from the solubility parameters by the equation

$$\chi_{ij} = \frac{V_{\mathrm{bead}}}{kT}(\delta_i - \delta_j)^2 \tag{7}$$

where V_{bead} is the arithmetic average of molar volumes of two beads; δ_i and δ_j are the solubility parameters of bead i and j, respectively. The values of solubility parameters depend on the chemical nature of species and can be obtained by molecular dynamics (MD) simulations.

Atomistic simulations were performed to calculate the solubility parameters and molar volumes of beads in this system. To optimize the geometries of the beads, successive applications of steepest descents, conjugate gradients, and Newton minimization methods for a total of 50 000 steps was applied in Materials Studio Program (Accelrys Inc.). MD simulations were performed using the Amorphous Cell module of the same program. Simulation boxes containing 50 beads of the same type were constructed. 50 ps MD simulations were performed to equilibrate the system at 298.15 K, followed by 500 ps MD simulations on these boxes. Periodic conditions were employed in the canonical ensemble (NVT). Initial velocities have been assigned from a Maxwell−Boltzmann distribution in such a way that the total momentum in all directions sums up to zero. Compass force field was used in geometry optimizations and MD simulations.[45]

In addition, a spring force ($\mathbf{F}_i^{\mathrm{S}}$) acts between beads which are connected in molecules. By means of this spring force, the particles can be interconnected to complex topologies. A simple harmonic force law is used for this force on particle i:

$$\mathbf{F}_i^{\mathrm{S}} = \sum_j C\mathbf{r}_{ij} \tag{8}$$

where C is the spring constant, and the sum runs over all particles to which particle i is connected.

3.2. Models and Interaction Parameters. The components being used in this work comprised of DOX, HR20-Chol, and water. The conformation of drug molecule may be fairly specific to the solvent, especially for macro-drug molecules (i.e., protein). Therefore, it is still difficult for DPD simulations to be used in protein delivery systems. For, DOX, a small molecule drug, the molecular conformation is not so much importance as that of proteins. Thus, simple coarse-grained bead−spring type models were used for the components in this study, as shown in Figure 1. The molecular structure of doxorubicin is divided into three types of beads (D1, D2, and D3). Three water molecules are represented as one bead W. Cholesterol segment is separated into three types of beads (C1, C2, and C3), histidine residue is divided into two types of beads (P and H), and arginine residue is divided into two types of beads (P and A). The histidine residue exists in different forms in different pH conditions as shown in Figure S1, Supporting Information. The bead of H was represented as H1 and H2 at pH > 6 and pH < 6, respectively. HR20-Chol is based on the linear bead−spring polymer chain representation. The calculated interaction parameters at 298.15 K used in this work are given in Table S1 of the Supporting Information. In addition, the hydrophobic interaction in this system is the main force which

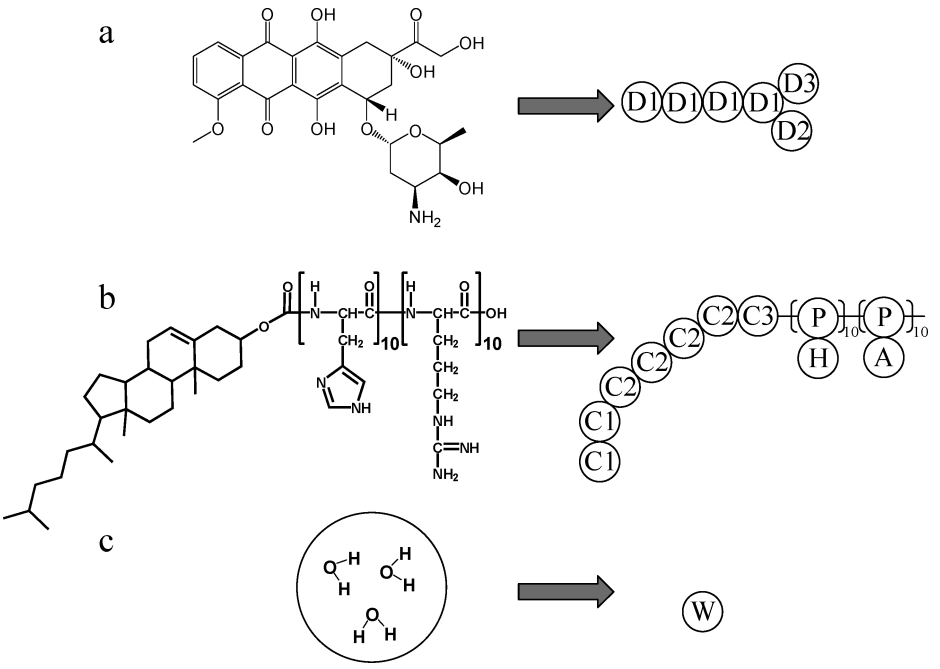

Figure 1. Coarse-grained models of (a) doxorubicin, (b) HR20-Chol, and (c) water.

leads to the segment flexibility. Thus, the simulation results were not very sensitive to the spring constant. In the current work, the spring constants between beads D1 and D1, C2, and C2 were set as 3, 4, and 5. Other spring constants were all set as 4. The density profiles of each segment in DOX loaded micelles at pH > 6.0 and pH < 6.0 did not change much, as shown in Figure S2, Supporting Information. Therefore, the packing in the core of the micelles was not very sensitive to the spring constant. In this study, the uniform spring constant of 4 was used, resulting in a slightly smaller distance for bonded beads than for nonbonded ones.

A cubic simulation box with periodic boundary condition was applied in all three directions. To avoid the finite size effects, DPD simulations were performed in $10 \times 10 \times 10$, $15 \times 15 \times 15$, $20 \times 20 \times 20$, $30 \times 30 \times 30$, and $40 \times 40 \times 40$ cubic box with 60 000 time steps. The system composed of 8% HR20-Chol, 2% DOX, and 90% water. The number-average diameters of the simulated particles in different box sizes are shown in Figure S3, Supporting Information. It can be found that the average diameter of simulated particles increases with the box size increasing when smaller box was adopted. However, the particle sizes are almost the same in 20, 30, and 40 boxes, indicating that a box of $20 \times 20 \times 20$ is sufficient to avoid the finite size effects. In this work, the box size of $30 \times 30 \times 30$ was used, which is large enough to avoid the finite size effects. The corresponding sizes of drug loaded or blank micelles are the optimum ones. The integration time step of 0.05 and simulation steps of 60 000 were used for our system to get thermodynamic equilibrium. In this work, the chosen particles have an average volume of 95 Å^3. Because the particle density is 3, a cube of r_c^3 contains three particles and therefore corresponding to a volume of 285 Å^3. Then we can find the physical size of the interaction radius, $r_c = 6.58$ Å. Thus, the box size in our work was characterized by effective dimensions of 197.4 Å × 197.4 Å × 197.4 Å, which can be used to calculate the length of the simulated structures. The main goal of this work is to study the microstructures of drug loaded micelles at different pH values. Although the size of particles in simulations could not quantitatively match the size in experiments, the structural transformation and drug distribution inside the micelles at different pH values could also be qualitatively predicted, from which one can compare the drug release profiles at different pH conditions.

Table 1. Flory−Huggins Interaction Parameters (χ) of Water and Other Components Computed from MD Simulations

	DOX	Chol	Arg	His (pH > 6)	His (pH < 6)
water	48.3	39.2	0.03	27.5	0.76

4. Results and Discussion

4.1. Interactions between Water and Other Segments. The Flory−Huggins theory was originally put forth to describe the miscibility of dilute polymer−solvent mixtures. In more recent years, Flory−Huggins theory has been successfully used to characterize the compatibility between small molecules, such as polymer−drug,[46,47] solvent−solvent,[48] and other mixtures.[49] Thus, this theory could also be applied in the compatibility studies of components in drug delivery systems. Besides the Flory−Huggins parameters between every two beads, the χ values for water and other segments were also calculated to investigate the interactions between water and other segments, as shown in Table 1. According to the Flory−Huggins solution theory, lower χ values indicate better solubility. For the Flory−Huggins parameters between same molecules, the χ value is 0. The critical χ value above which a polymer and a solvent become immiscible is 0.5. In other words, if χ value is lower than 0.5 or is negative, then they are soluble into each other. However, because the theory is mainly developed for a solvent and polymer that mainly interact through nonpolar dispersion forces. The use of 0.5 for our system, which involve both Coulombic and hydrogen-bonding interactions, is not suitable. Therefore, we judge whether compatibility prediction is successful by comparing the trend of the computed interaction parameters from MD simulations. It can be found from Table 1 that the repulsion between water and DOX is the strongest one in this system. Furthermore, the repulsion between water and cholesterol is also very strong, while the repulsion between water and arginine is very weak. The combined interactions could lead to the micelle formation of HR20-Chol in aqueous solution. This

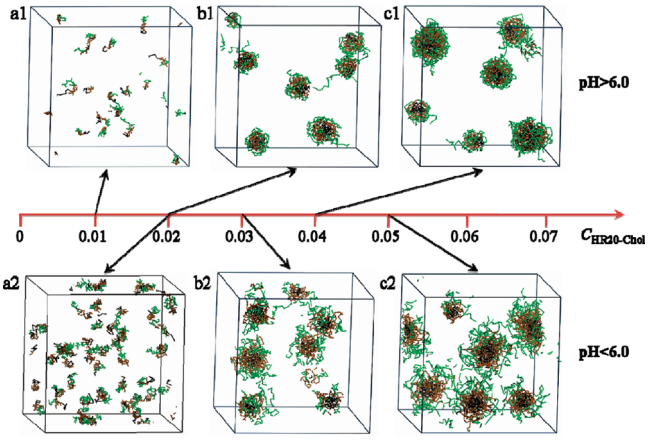

Figure 2. Typical simulated snapshots of HR20-Chol in aqueous solution at pH > 6.0 (a1, b1, and c1) and pH < 6.0 (a2, b2, and c2). The green, brown, and black lines represent arginine, histidine, and cholesterol, respectively. Water is omitted. The same symbols are used in the following figures.

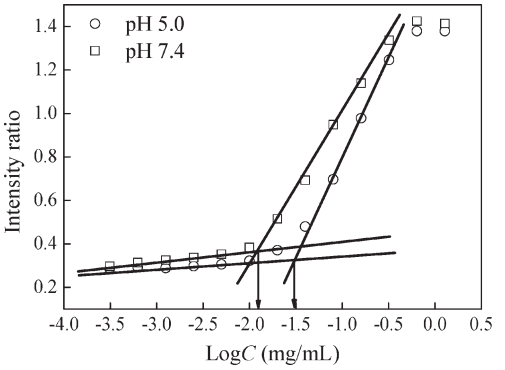

Figure 3. A graph of intensity ratio (i.e., I_{339} to I_{334}) as a function of logarithm of HR20-Chol concentrations in aqueous solution with different pH values.

micelle has core/shell architecture that is composed of hydrophobic cholesterol and hydrophilic arginine residues. For the interaction between water and histidine, the χ value is 27.5 and 0.76 at pH > 6.0 and pH < 6.0, respectively. Thus, histidine residue exhibits hydrophobic performance at pH > 6.0 and hydrophilic at pH < 6.0. This could attribute to the conversion of nonionized histidine residue to ionized one by the protonation of imidazole group.

4.2. Micelle Formation of Cholesterol Conjugated Peptides. When the amphiphilic copolymer concentration in water is higher than the critical micellization concentration (CMC), micelles start to form. In the present study, the conformations of HR20-Chol in aqueous solution with different concentrations were investigated. With an increase of the concentration of HR20-Chol ($C_{HR20\text{-}Chol}$), spherical micelles start to form at defined concentrations. The typical simulated results for HR20-Chol are shown in Figure 2. All the simulations were start from homogeneous states. The volume concentration of typical spherical micelles formed was around 0.02% and 0.03% for HR20-Chol at pH > 6.0 and pH < 6.0, respectively. The CMC value is higher at pH < 6.0 than that of pH > 6.0. With the decrease of pH from pH > 6.0 to pH < 6.0, the histidine residues are conversed to ionized ones by the protonation of imidazole groups. This conversion of nonionized histidine residues to hydrophilic ones should be responsible for the higher CMC values. To verify the correctness of the simulated results, experiments were also performed to characterize the CMC values for this conjugate at pH 5.0 and pH 7.4, which are shown in Figure 3. The experimental CMC results could not quantitatively consistent with the values from simulations due to the coarse-graining of components. However, they are consistent with the simulation results qualitatively. All the results confirmed the important role of pH value in micelle formation process. The higher pH value can facilitate the formation of micelles.

4.3. Drug Loading and Distribution in Micelles. It is known that the hydrophobic core of micelles can provide a loading space for hydrophobic drugs (e.g., DOX). To evaluate the drug loading abilities of micelles at different pH conditions, the conformations of drug-loaded HR20-Chol micelles in aqueous solution with different DOX concentrations (C_{DOX}) were investigated, as shown in Figure S4, Supporting Information. The system composed of 7% HR20-Chol. The value of C_{DOX} was scanned from 0 to 7% with the step of 0.2%. All the simulations were started from homogeneous states. When C_{DOX} is zero, blank micelles were formed at both pH conditions. With the increase of C_{DOX}, DOX molecules were efficiently encapsulated in micelles. At pH > 6.0, when C_{DOX} exceeds 5%, some DOX molecules could not be encapsulated in micelles. At pH < 6.0, the micelles could only load about 2.8% of DOX. At pH < 6.0, the histidine residues are hydrophilic ones which cannot facilitate loading drugs, leading to a lower drug loading ability as compared to the micelles formed at pH > 6.0.

In order to gain an insight of the drug distribution inside the micelles, the system composed of 7% HR20-Chol, 3% DOX, and 90% water was further analyzed. The simulated results at pH > 6.0 and pH < 6.0 are shown in Figure 4a,c. At pH > 6.0, all the DOX molecules were encapsulated inside the micelles. From the section view of one micelle, three layers can be observed. Most DOX molecules distribute in the cholesterol core of the micelle. Some DOX molecules also distribute inside the histidine middle layer of the micelle. Arginine residues distribute on the surface of the micelle, which can prevent DOX molecules escaping from the core of the micelle. Figure 4b shows the density profiles of DOX, histidine, arginine, and cholesterol segments in the micelle. Three layers can be easily observed from the density profiles of each segment. The core of the micelle is composed of cholesterol and DOX, the middle layer is histidine segment, and the shell is arginine segment. At pH < 6.0, some DOX molecules cannot be encapsulated inside the micelles, leading to a lower DOX loading ability of micelles due to the hydrophilicity of histidine residue. From the section view of one micelle in the simulated results, DOX distribute inside the core of the micelle. Compared with the dense structure of DOX-loaded micelles formed at pH > 6.0, the structure of micelles formed at pH < 6.0 exhibits swollen conformation. From the density profiles of each segment (Figure 4d), the histidine and arginine layers trend to be mixing together. The core of the micelle is composed of cholesterol segment and DOX, and the shell of the micelle is composed of histidine and arginine segments. This difference could attribute to the transformation of histidine residues from hydrophobic to hydrophilic ones when pH decreases from pH > 6.0 to pH < 6.0.

4.4. Effects of pH on Microstructures of Micelles. To further investigate the pH-sensitivity of the micelles, the micellar kinetic structural transformation was studied. Figure 5 shows the micelles formation and the structural transformation from pH > 6.0 to pH < 6.0. At pH value higher than 6.0, the cholesterol conjugated peptides form core/shell micelles from homogeneous state. Cholesterol and histidine segments form the cores of the micelles and are surrounded by the arginine shell. The structure of micelles shows dense conformation due to the

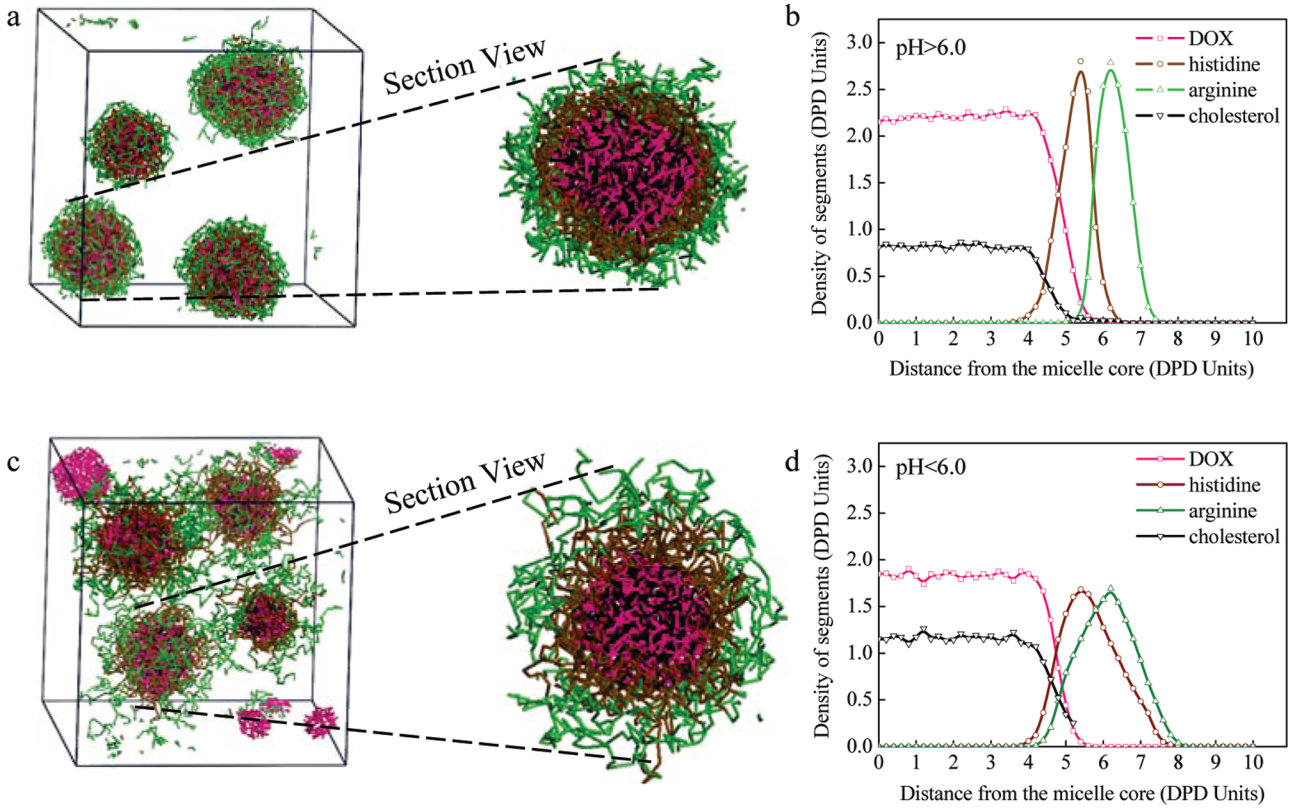

Figure 4. Typical simulated snapshots and section view of DOX loaded micelles at (a) pH > 6.0 and (c) pH < 6.0. (b) and (d) are the density profiles of each segment at pH > 6.0 and pH < 6.0, respectively. DOX is drawn in pink.

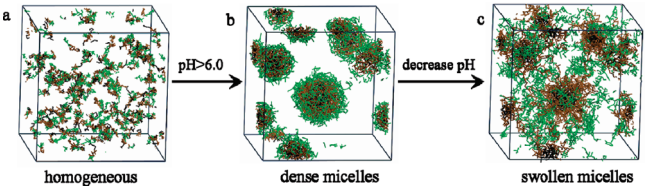

Figure 5. Kinetic HR20-Chol micelles formation from (a) homogeneous state at pH > 6.0 and the structural transformation of the micelles from (b) pH > 6.0 to (c) pH < 6.0.

hydrophobicity of histidine segment. As the pH value decreased to lower than 6.0, the structure of the micelles trends to be swelling. The dynamic process of the micelles formation and the structural transformation can be clearly seen in Video S1 of the Supporting Information. This structural transformation was caused by the protonation of imidazole groups in histidine residues at lower pH conditions. This swollen micellar structure can provide channels for drug diffuse, facilitating the release of DOX at lower pH conditions. To verify the pH-sensitivity of micelles from the simulated results, experiments were also performed to characterize the DOX release behavior at pH 5.0 and pH 7.4. A low concentration would dissolve the micelles and instantaneously release the drugs. To avoid this effect, the drug release experiments were performed with the concentration of 1 mg/mL, which is much higher than the CMC of HR20-Chol (28 and 12 mg/L at pH 5.0 and 7.4, respectively). The *in vitro* drug release profiles are shown in Figure 6. It was observed that the release rate of DOX from the micelles is influenced by pH values. At pH 7.4, the drug molecules cannot release drastically from micelles due to the dense conformation of micelles. When the pH is lower than 6.0, the drug release rate is markedly accelerated, which are consistent with the simulation results qualitatively.

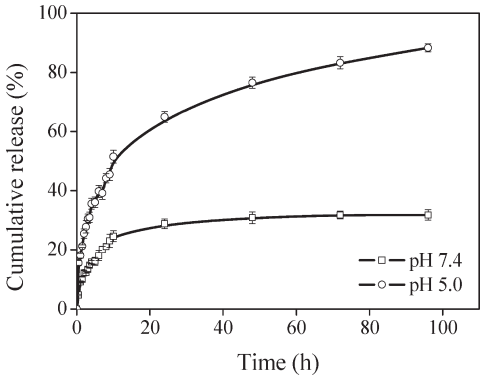

Figure 6. *In vitro* drug release profiles from DOX loaded micelles self-assembled from HR20-Chol at pH 7.4 and 5.0 PBS solutions at 37 °C.

5. Conclusions

Through computer simulations on the DOX-loaded HR20-Chol system based on atomistic simulations, Flory−Huggins parameters between water and other components were calculated. The repulsions between water and DOX, water, and cholesterol are very strong. For the interaction between water and histidine, the χ value is much higher at pH > 6.0 (27.5) than that at pH < 6.0 (0.76), leading to the pH-sensitivity of histidine residues. In addition, the microstructures of DOX-loaded and blank micelles at different pH conditions have been intuitively reproduced by DPD simulations. DOX molecules could be loaded inside the core of micelles. The density profiles of each segments in this system were calculated which clearly showed the microstructure of DOX load micelles. At pH > 6.0, these micelles has a stronger DOX loading ability due to the hydrophobicity of histidine residues. At pH values lower than 6.0, the dense structures of micelles transform into swollen conformations. This structural transformation

can markedly accelerate the drug release. All the simulation results are consistent with the experimental results qualitatively, indicating that the DPD method is a powerful tool for designing drug delivery systems.

Acknowledgment. This work was financially supported by National Natural Science Foundation of China (No. 20536020 and No. 20776049), Guangdong Province Science Foundation (No. 9251064101000009), and State Key Laboratory of Chemical Engineering (No. SKL-ChE-09A04), and Guangzhou Municipal Bureau of Science and Technology (No. 2009J1-C511-2). We thank Prof. G. S. Luo and Prof. Z. Liu of Tsinghua University for valuable discussions.

Supporting Information Available: Figures S1−S4, Table S1, and Video S1. This material is available free of charge via the Internet at http://pubs.acs.org.

References and Notes

(1) Shen, Y.; Zhan, Y.; Tang, J.; Xu, P.; Johnson, P. A.; Radosz, M. *AIChE J.* **2008**, *54* (11), 2979–2989.
(2) Li, Y. Y.; Zhang, X. Z.; Cheng, H.; Kim, G. C.; Cheng, S. X.; Zhuo, R. X. *Biomacromolecules* **2006**, *7* (11), 2956–2960.
(3) Wei, L.; Cai, C.; Lin, J.; Chen, T. *Biomaterials* **2009**, *30* (13), 2606–2613.
(4) Zhang, X.; Hua, W.; Cheng, C.; Cheng, S. X.; Zhuo, R. X. *Biomaterials* **2007**, *28* (1), 99–107.
(5) Kim, D.; Lee, E. S.; Oh, K. T.; Gao, Z. G.; Bae, Y. H. *Small* **2008**, *4* (11), 2043–2050.
(6) Hruby, M.; Konak, C.; Ulbrich, K. *J. Controlled Release* **2005**, *103*, 137–148.
(7) Liu, J.; Zhang, L.; Lam, J. W. Y.; Jim, C. K. W.; Yue, Y.; Deng, R.; Hong, Y.; Qin, A.; Sung, H. H. Y.; Williams, I. D.; Jia, G.; Tang, B. Z. *Macromolecules* **2009**, *42* (19), 7367–7378.
(8) Langer, R.; Peppas, N. A. *AIChE J.* **2003**, *49* (12), 2990–3006.
(9) Soppimath, K. S.; Liu, L. H.; Seow, W. Y.; Liu, S. Q.; Powell, R.; Chan, P.; Yang, Y. Y. *Adv. Funct. Mater.* **2007**, *17* (3), 355–362.
(10) Li, Y. Y.; Zhang, X. Z.; Cheng, H.; Zhu, J. L.; Cheng, S. X.; Zhuo, R. X. *Macromol. Rapid Commun.* **2006**, *27* (22), 1913–1919.
(11) Abdekhodaie, M. J.; Wu, X. Y. *Biomaterials* **2008**, *29* (11), 1654–1663.
(12) Lin, J.; Zhu, J.; Chen, T.; Lin, S.; Cai, C.; Zhang, L.; Zhuang, Y.; Wang, X.-S. *Biomaterials* **2008**, *30* (1), 108–117.
(13) Schmaljohann, D. *Adv. Drug Delivery Rev.* **2006**, *58* (15), 1655–1670.
(14) Srinivas, G.; Discher, D. E.; Klein, M. L. *Nature Mater.* **2004**, *3* (9), 638–644.
(15) Wong-Ekkabut, J.; Baoukina, S.; Triampo, W.; Tang, I.-M.; Tieleman, D. P.; Monticelli, L. *Nature Nanotechnol.* **2008**, *3*, 363–368.
(16) Marrink, S. J.; Mark, A. E. *J. Am. Chem. Soc.* **2003**, *125* (49), 15233–15242.
(17) Fedosov, D. A.; Karniadakis, G. E.; Caswell, B. *J. Chem. Phys.* **2008**, *128* (14).
(18) Ortiz, V.; Nielsen, S. O.; Discher, D. E.; Klein, M. L.; Lipowsky, R.; Shillcock, J. *J. Phys. Chem. B* **2005**, *109* (37), 17708–17714.
(19) Fermeglia, M.; Longo, G.; Toma, L. *AIChE J.* **2009**, *55* (4), 1056–1064.
(20) Chen, P.; Liang, H.; Shi, A.-C. *Macromolecules* **2008**, *41* (22), 8938–8943.
(21) Li, X.; Pivkin, I. V.; Liang, H.; Karniadakis, G. E. *Macromolecules* **2009**, *42* (8), 3195–3200.
(22) Qian, H. J.; Lu, Z. Y.; Chen, L. J.; Li, Z. S.; Sun, C. C. *Macromolecules* **2005**, *38* (4), 1395–1401.
(23) Ankola, D. D.; Durbin, E. W.; Buxton, G. A.; Schafer, J.; Bakowsky, U.; Kumar, M. N. V. R. *Nanotechnology* **2010**, *21* (6).
(24) Buxton, G. A.; Clarke, N. *Soft Matter* **2007**, *3* (12), 1513–1517.
(25) Durbin, E. W.; Buxton, G. A. *Soft Matter* **2010**, *6* (4), 762–767.
(26) Hoogerbrugge, P. J.; Koelman, J. *Europhys. Lett.* **1992**, *19* (3), 155–160.
(27) Espanol, P.; Warren, P. *Europhys. Lett.* **1995**, *30* (4), 191–196.
(28) Koelman, J.; Hoogerbrugge, P. J. *Europhys. Lett.* **1993**, *21* (3), 363–368.
(29) Groot, R. D.; Madden, T. J. *J. Chem. Phys.* **1998**, *108* (20), 8713–8724.
(30) Groot, R. D.; Warren, P. B. *J. Chem. Phys.* **1997**, *107* (11), 4423–4435.
(31) Dong, F. L.; Li, Y.; Zhang, P. *Chem. Phys. Lett.* **2004**, *399* (1−3), 215–219.
(32) Khokhlov, A. R.; Khalatur, P. G. *Chem. Phys. Lett.* **2008**, *461* (1−3), 58–63.
(33) Yan, L.-T.; Zhang, X. *Soft Matter* **2009**, *5* (10), 2101–2108.
(34) Liu, D. H.; Zhong, C. L. *Macromol. Rapid Commun.* **2007**, *28* (3), 292–297.
(35) Xin, J.; Liu, D.; Zhong, C. *J. Phys. Chem. B* **2009**, *113* (28), 9364–9372.
(36) Xin, J.; Liu, D.; Zhong, C. L. *J. Phys. Chem. B* **2007**, *111* (49), 13675–13682.
(37) Liu, D. H.; Zhong, C. L. *Macromol. Rapid Commun.* **2006**, *27* (6), 458–462.
(38) Loverde, S. M.; Ortiz, V.; Kamien, R. D.; Klein, M. L.; Discher, D. E. *Soft Matter* **2010**, *6* (7), 1419–1425.
(39) Ginzburg, V. V.; Balijepailli, S. *Nano Lett.* **2007**, *7* (12), 3716–3722.
(40) Guo, X. D.; Zhang, L. J.; Qian, Y.; Zhou, J. *Chem. Eng. J.* **2007**, *131* (1−3), 195–201.
(41) Guo, X. D.; Tan, J. P. K.; Zhang, L. J.; Khan, M.; Liu, S. Q.; Yang, Y. Y.; Qian, Y. *Chem. Phys. Lett.* **2009**, *473* (4−6), 336–342.
(42) Guo, X. D.; Tan, J. P. K.; Kim, S. H.; Zhang, L. J.; Zhang, Y.; Hedrick, J. L.; Yang, Y. Y.; Qian, Y. *Biomaterials* **2009**, *30* (33), 6556–6563.
(43) Guo, X. D.; Zhang, L. J.; Chen, Y.; Qian, Y. *AIChE J.* **2010**, *56* (7), 1922–1931.
(44) Guo, X. D.; Tandiono, F.; Wiradharma, N.; Khor, D.; Tan, C. G.; Khan, M.; Qian, Y.; Yang, Y.-Y. *Biomaterials* **2008**, *29* (36), 4838–4846.
(45) Sun, H. *J. Phys. Chem. B* **1998**, *102* (38), 7338–7364.
(46) Patel, S.; Lavasanifar, A.; Choi, P. *Biomacromolecules* **2008**, *9* (11), 3014–3023.
(47) Pajula, K.; Taskinen, M.; Lehto, V.-P.; Ketolainen, J.; Korhonen, O. *Mol. Pharmaceutics* **2010**, *7* (3), 795–804.
(48) Sreekanth, T. V. M.; Reddy, K. S. *Chromatographia* **2007**, *65* (5−6), 325–330.
(49) Merino-Garcia, D.; Correra, S. *J. Dispersion Sci. Technol.* **2007**, *28* (3), 339–347.